ELSEVIER

Journal of Structural Geology 28 (2006) 1725–1733

JOURNAL OF STRUCTURAL GEOLOGY

www.elsevier.com/locate/jsg

Divergent and convergent non-isochoric deformation

Marcus Ebner*, Bernhard Grasemann

Department of Geodynamics and Sedimentology, Structural Processes Group, University of Vienna, Althanstrasse 14, A-1090 Vienna, Austria

Received 9 March 2006; received in revised form 19 June 2006; accepted 11 July 2006
Available online 1 September 2006

Abstract

Plane strain flow with zero elongation parallel to, but widening, or shortening perpendicular to the flow plane results in either divergent or convergent non-isochoric deformation. During this special type of flow the kinematic dilatancy number, a measure of the rate at which a surface changes area with time, is directly dependent on the kinematic vorticity number, a measure of the rotational quality of a flow type, and vice versa. Thus, the velocity gradients' tensor can be simplified being only defined by the vorticity and the instantaneous area change. If these numbers can be deduced from natural deformed rocks with the help of quantitative kinematic indicators, the finite deformation can be calculated if the volume change is known from independent criteria. We quantitatively examine a marble mylonite from the Tauern Window, which deformed by stress-induced solution mass transfer that exhibits convergent non-isochoric deformation.

Keywords: Non-isochoric flow; Volumetric strain; Dilatation; Kinematic modeling; Velocity gradients tensor; Stylolites

1. Introduction

The geometry of structures in deformed rocks is a function of the perturbation flow field imposed on the material during deformation (Passchier et al., 2005). One of the primary aims of structural geology is to use structures from naturally deformed rocks in order to reconstruct the flow. Theoretical studies of deformed rocks frequently assume plane strain and homogeneous deformation composed of combinations of pure and simple shear. Quantitative kinematic studies of naturally sheared rocks have shown that shear zones, frequently record a layer-normal thinning and layer-parallel stretching component (e.g. Lister and Williams, 1983; Platt and Behrmann, 1986; Passchier, 1987, 1988; Vissers, 1989; Wallis, 1992, 1995; Druguet et al., 1997; Simpson and De Paor, 1997; Grasemann et al., 1999; Holcombe and Little, 2001; Law et al., 2004; Carosi et al., 2006) and have therefore been deformed by general shear. All of these studies rely on conservation of volume during progressive deformation. However, naturally deformed rocks often record microstructures such as stylolites, pressure solution seams, crenulation cleavage or preferential dissolution around rigid clasts, all of which result from mass transfer processes and associated volume change during deformation. Several studies suggest possible volume change during deformation (e.g. Schwerdtner, 1982; Wright and Platt, 1982; Ring, 1998; Ring et al., 2001; Sturm, 2003) but kinematic studies typically focus on area change with an isotropic change in all line lengths (e.g. Passchier, 1988, 1991). However, mass transfer processes, which are probably associated with non-isochoric deformation, can strongly modify the eigenvectors of flow (Grasemann et al., 2006). This study focuses on plane strain flow associated with non-isochoric deformation where there is zero elongation parallel to the flow plane. Such a deformation is here defined as divergent or convergent non-isochoric deformation (Marrett and Peacock, 1999). We firstly derive the velocity and deformation gradients tensors discussing some fundamental properties and possible geological scenarios. Secondly, we quantitatively investigate a natural example from a marble shear zone, which experienced post-mylonitic convergent non-isochoric deformation by stress-induced solution mass transfer processes.

2. Kinematic model

We investigate the kinematic consequences of plane strain, non-isochoric, homogeneous deformation with zero elongation

* Corresponding author. Tel.: +43 1 4277 53442; fax: +43 1 4277 9534.
E-mail address: marcus.ebner@univie.ac.at (M. Ebner).

0191-8141/$ - see front matter © 2006 Elsevier Ltd. All rights reserved.
doi:10.1016/j.jsg.2006.07.008

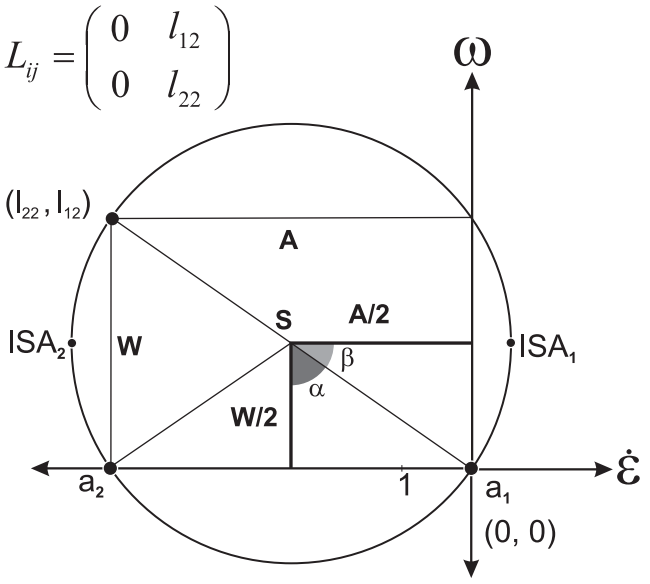

Fig. 1. Mohr circle for the velocity gradients tensor $\boldsymbol{L}$ for convergent non-isochoric flow. $ISA_{1,2}$ – instantaneous stretching axes; $a_{1,2}$ – eigenvectors; W – vorticity; A – instantaneous area change; S – differential stretching rate. Note the Pythagorean relationship between W and A.

parallel to the shearing plane. We consider the special case, where the area change due to shortening or widening perpendicular to the shear zone boundary is not balanced by elongation parallel to the flow plane. Because the model is restricted to two-dimensions, we investigate the effects of non-isochoric deformation in sections parallel to the flow direction. In particular, we investigate flow types that record zero elongation parallel to the flow plane. This flow geometry occurs for example in shear zones where the dominant deformation mechanism is solution mass transfer and where a pronounced shortening normal to the shear zone is balanced by mass-loss volume strains (Ring et al., 2001) or during processes of compaction (Ramsay and Huber, 1983, 1987).

Non-isochoric flow has been investigated by means of the velocity gradients tensor $\boldsymbol{L}$ (Passchier, 1988, 1991). The Eulerian rate of displacement is defined by:

$$\dot{X}_{ij} = \boldsymbol{L}_{ij} X_j \tag{1}$$

where $\boldsymbol{L}$ is the velocity gradients tensor and X the spatial position of a particle. The column vectors of $\boldsymbol{L}$ can be used to construct a Mohr circle (De Paor and Means, 1984) by plotting stretching rate $\dot{\varepsilon}$ against the angular velocities ω of material lines (Fig. 1). The coordinates of the centre of the Mohr circle represent half of the instantaneous area change A (equivalent to a in Passchier, 1988) and half of the vorticity W (Passchier, 1991). In isochoric flow types, $A = 0$ and therefore the Mohr circle is centred on the ordinate. The intersection of the Mohr circle with the $\dot{\varepsilon}$-axis represent eigenvectors of $\boldsymbol{L}$ (a_1 and a_2), which are lines of no instantaneous angular velocities (Bobyarchick, 1986). The cosine of the angle α between the eigenvectors gives the kinematic vorticity number W_k (Truesdell, 1954):

$$\cos\alpha = W_k = \frac{W}{S} \tag{2}$$

where S is the differential stretching rate or the diameter of the Mohr circle. This term is twice the mean instantaneous stretching rate of Passchier (1988) or the deviatoric strain rate intensity used by Lister and Williams (1983). As a consequence, a shift of the centre of the Mohr circle along the ordinate (ω-axis in Mohr space) reflects a change of W and therefore a change of W_k (Fig. 2a). By analogy with W_k, the kinematic dilatancy number A_k (Passchier, 1988, 1991) is defined as the cosine of β, which is half the angle subtended at the centre of the Mohr circle by the points of intersection with the ordinate (Fig. 1):

$$\cos\beta = A_k = \frac{A}{S} \tag{3}$$

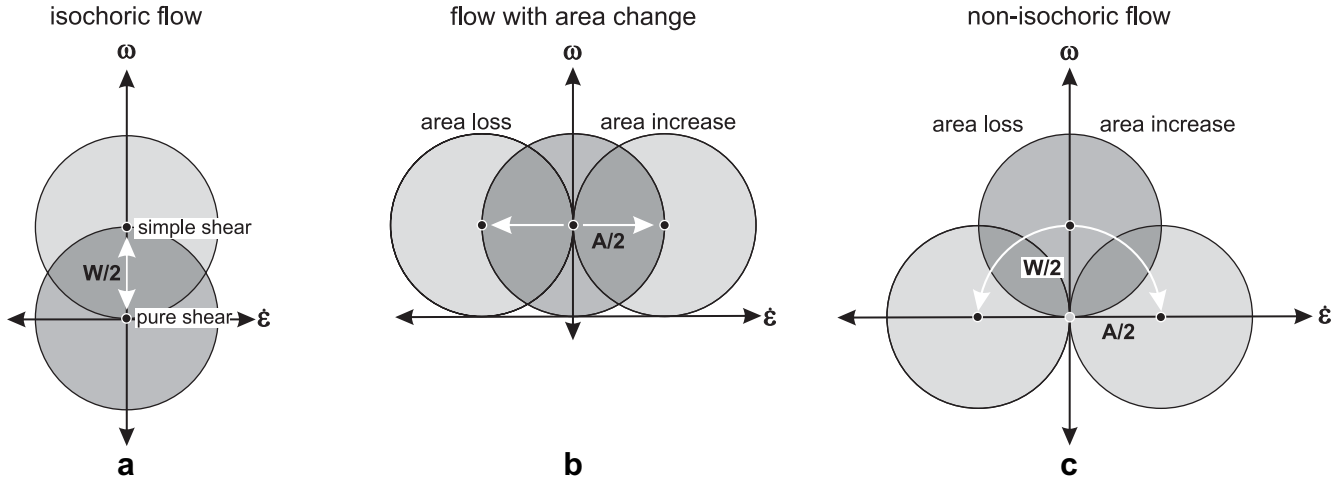

Fig. 2. Mohr circles for the velocity gradients tensor $\boldsymbol{L}$ for: (a) isochoric flow; (b) flow with area change; (c) convergent/divergent non-isochoric flow with no elongation parallel to the flow plane. Subject of this study is flow type c.

Non-isoplanar flow (Passchier, 1988), which implies an area change as a result of an isotropic change in all line lengths, results in a translation of the centre of the Mohr circle of the velocity gradients tensor parallel to the abscissa but $W/2$ and S and therefore also W_k are unaffected (Fig. 2b). $\boldsymbol{L}$ can be defined in terms of W_k, S and A_k (modified after Passchier, 1988):

$$\boldsymbol{L}_{ij} = \begin{pmatrix} \frac{S}{2}\left(A_k + \sqrt{1-W_k^2}\right) & SW_k \\ 0 & \frac{S}{2}\left(A_k - \sqrt{1-W_k^2}\right) \end{pmatrix} \quad (4)$$

The deformation considered in this work is the result of non-isochoric flow, which is a more general term meaning any flow that changes area in two-dimensions (or volume in three-dimensions). A non-isochoric flow could change W, S, and/or W_k. Here, we furthermore allow zero elongation in the flow plane and therefore a_1 is located at the origin of the $\dot{\varepsilon}$–ω-coordinate system (Fig. 2c). Non-isochoric flow results in a clockwise or anticlockwise rotation of the Mohr circle around a_1, respectively. Both W_k and A_k are modified by this flow type because of the Pythagorean relationship of S, W and A, A_k is directly dependent on W_k:

$$A_k = \pm\sqrt{1-W_k^2} \quad (5)$$

If the flow is simple shearing ($W_k = \pm 1$) and $A_k = 0$, there is no area change. If a rock volume is deformed with coaxial deformation ($W_k = 0$), and $A_k = \pm 1$ therefore the whole deformation is balanced by non-isochoric deformation. Substituting Eqs. (2), (3) and (5), Eq. (4) simplifies to:

$$\boldsymbol{L}_{ij} = \begin{pmatrix} A & W \\ 0 & 0 \end{pmatrix} \quad (6a)$$

or:

$$\boldsymbol{L}_{ij} = \begin{pmatrix} 0 & W \\ 0 & A \end{pmatrix} \quad (6b)$$

Eq. (6a) describes deformation where the shear zone has a constant thickness. A non-isochoric flow regime forces elongation parallel to the flow plane. Positive elongation is associated with $A > 0$ resulting in an extrusion type flow (Fig. 3a, see also Grasemann et al., 2006). Negative elongation is associated with $A < 0$ (Fig. 3b). Here we focus on Eq. (6b) with constant length of material lines parallel to the flow plane resulting in either divergent transcurrence ($A > 0$, Fig. 3c) or convergent transcurrence ($A < 0$, Fig. 3d, see also Marrett and Peacock, 1999). $\boldsymbol{L}$ can be easily converted into the finite Lagrangian deformation tensor $\boldsymbol{D}$, given that $0 \leq |W_k| < 1$ (Ghosh and Ramberg, 1976; Provost et al., 2004):

$$\boldsymbol{D}_{ij} = \exp\left(\boldsymbol{L}_{ij} t\right) \quad (7)$$

Therefore $\boldsymbol{L}$ from Eq. (6b) representing non-isochoric deformation with zero elongation parallel to the flow plane is given over a time increment (t) of 1:

$$\boldsymbol{D}_{ij} = \begin{pmatrix} 1 & \frac{W(e^A - 1)}{A} \\ 0 & e^A \end{pmatrix} \quad (8)$$

3. Divergent and convergent non-isochoric deformation

W_k is uniquely specified by the angle between the lines of no instantaneous rotation (Simpson and De Paor, 1997), which are symmetrically oriented to other important kinematic directions (e.g. instantaneous stretching axes, lines of maximum and minimum instantaneous rotations and shear strain rates), which control the formation of structures in rocks (e.g.

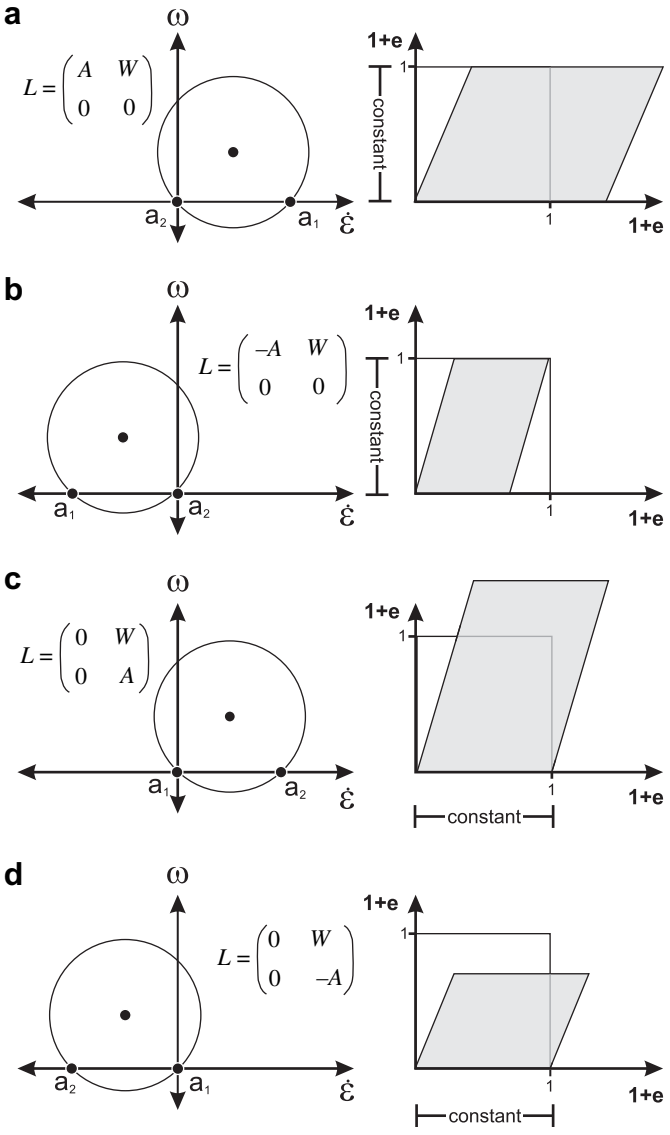

Fig. 3. Mohr circle for the velocity gradients tensor L with corresponding deformed unit square in physical space for: (a) constant thickness non-isochoric deformation with positive elongation parallel to the flow plane; (b) constant thickness non-isochoric deformation with negative elongation parallel to the flow plane; (c) divergent non-isochoric deformation with no elongation parallel to the flow plane; (d) convergent non-isochoric deformation with no elongation parallel to the flow plane. Subject of this study are flow types c and d.

extension gashes, dissolution seams, co-/counter shearing, co-/counter rotation, and stable/unstable orientations of markers).

Convergent and divergent non-isochoric flow significantly changes W_k as a function of A_k and therefore it is interesting to investigate $\boldsymbol{D}$ of this flow type in more detail (Grasemann et al., 2006). The special case of zero elongation parallel to the flow plane a_1 has two important consequences: (i) a_1 is located in the origin of the coordinate system in the Mohr space. (ii) According to Eq. (5) W_k, is directly related with A_k and is decreasing with increasing A_k. In the following we investigate the effects of interdependent change of W_k and A_k on the effective shear strain Γ (Fossen and Tikoff, 1993; Tikoff and Fossen, 1993) and the area change ΔA given in percent volume change for different finite bulk deformations. Note that, although we focus on the discussion of natural examples with volume loss, the equations are equally valid for non-isochoric deformation with area increase and zero elongation parallel to the flow plane.

Substituting Eq. (5) in Eq. (8), Γ (i.e. $\boldsymbol{D}_{12}$) can be plotted as a function of W_k for different S (Fig. 4a). Positive and negative sign control area increase (dotted lines in Fig. 4) and decrease (solid lines in Fig. 4), respectively:

$$\Gamma = \frac{\pm W_k \left(e^{\pm S\sqrt{1-W_k^2}} - 1 \right)}{\sqrt{1-W_k^2}} \tag{9}$$

For area loss, Γ increases/decreases exponentially with increasing/decreasing W_k reaching its limit and maximum/minimum in $W_k = \pm 1$, where $\Gamma = \pm S$ (Fig. 4a; dextral shear is defined as being positive). For area increase, the results are less intuitive: Again, $\Gamma = 0$ at $W_k = 0$ and reaches its limit in $W_k = \pm 1$, where $\Gamma = \pm S$. However, with increasing S, the maximum of Γ shifts towards lower W_k. Whereas the variation in Γ for area loss is only significant at higher strain ($S > 2$) and simple shear dominated flows ($W_k > \pm 0.8$), deformation associated with area increase reveal a sensitive change of Γ with changing W_k at higher strain. Note that a single value of Γ (e.g. 4 in Fig. 4a) could be characteristic for flows with different W_k (e.g. $W_k \sim 0.2$ and 0.9 in Fig. 4a).

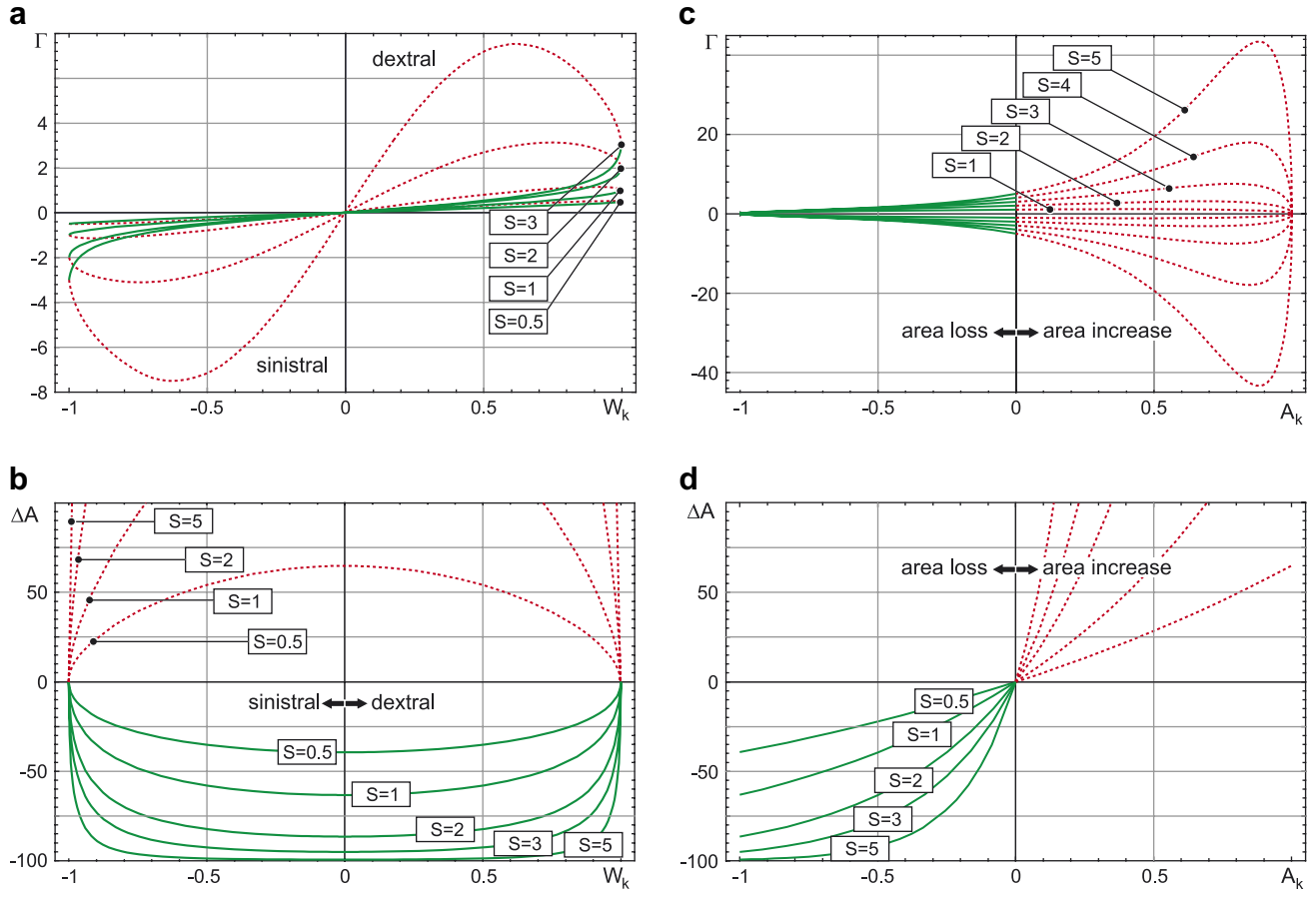

Fig. 4. Plot of different kinematic parameters for convergent/divergent non-isochoric deformation. Sinistral and dextral shear have a negative and positive W_k, respectively. Solid (green) and dotted (red) curves depict area loss and increase respectively. (a) Plot of kinematic vorticity number W_k versus effective shear strain Γ for various differential stretching rates S. Note, if $W_k = \pm 1$, $\Gamma = \pm S$. (b) Plot of kinematic vorticity number W_k versus percent area change ΔA for various differential stretching rates S. (c) Plot of kinematic dilatancy number A_k versus effective shear strain Γ for various differential stretching rates S. (d) Plot of kinematic dilatancy number A_k versus percent area change ΔA for various differential stretching rates S. Note that for area loss the curves have a limit in -100% ΔA.

Because W_k is directly related to A_k (Eq. (5)), ΔA (i.e. $\boldsymbol{D}_{22}$) can be plotted in percent area change as a function of W_k for different S (Fig. 4b). Again, the positive and negative sign controls area increase and decrease, respectively:

$$\Delta A = e^{\pm S\sqrt{1-W_k^2}} \tag{10}$$

Generally, the variation of ΔA is much more sensitive to a change in W_k at simple shear dominated flows, where $\Delta A = 0$ when W_k approaches ± 1. Therefore, an estimate of the area change might be a good proxy for estimating S in pure shear dominated flows. If area is lost during deformation, then ΔA equals the exponent of $-S$ and is a minimum at $W_k = 0$ having its limit at -100%. Deformation with area increase has no upper limits in ΔA mathematically, which has its maximum at $W_k = 0$ equalling the exponent of S. However, a physical limit will exist during natural deformation because an area increase during plane straining requires a decreasing rock density.

Rearranging Eq. (5), Γ and ΔA can be also plotted as a function of A_k (Fig. 4c and d). This rearrangement does not reveal any new relationships because of the direct dependence of A_k and W_k. Nevertheless, the plots show some interesting properties on non-isochoric deformation with zero elongation parallel to the flow plane. The effective shear strain can be expressed as a function of A_k and S (Fig. 4c):

$$\Gamma = \frac{\pm\sqrt{1-A_k^2}(e^{A_k S}-1)}{A_k} \tag{11}$$

Similarly to Fig. 4a, A_k approaches zero if Γ equals $\pm S$ and deformations with area loss reveal a dramatic lower degree dependence of Γ on A_k. The function has its limit in zero when A_k approaches ± 1. Because W_k changes along a curve

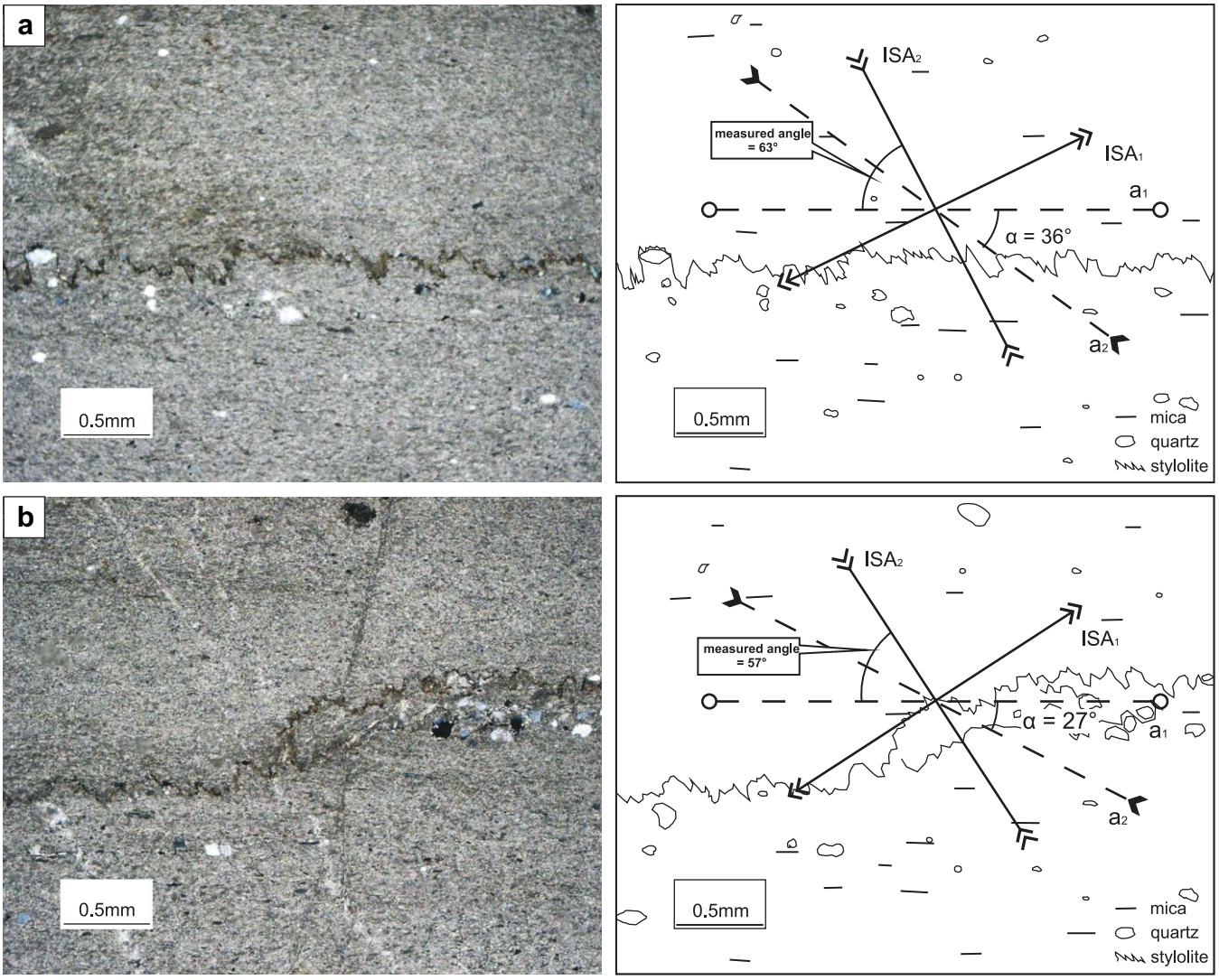

Fig. 5. Photomicrographs (left column) and line drawings (right column) of impure marble ultra-mylonites from the western Tauern Window that were used for the reconstruction of flow parameters (UTM 32 coordinates: Easting: 698 927 m Northing: 5 214 718 m, view to S). Slickolites suggest deformation by solution mass transfer. The long axes of the slickolite teeth make an angle of (a) 63° and (b) 57° with the solution surface, which is sub-parallel to the mylonitic foliation. For further explanation, see text.

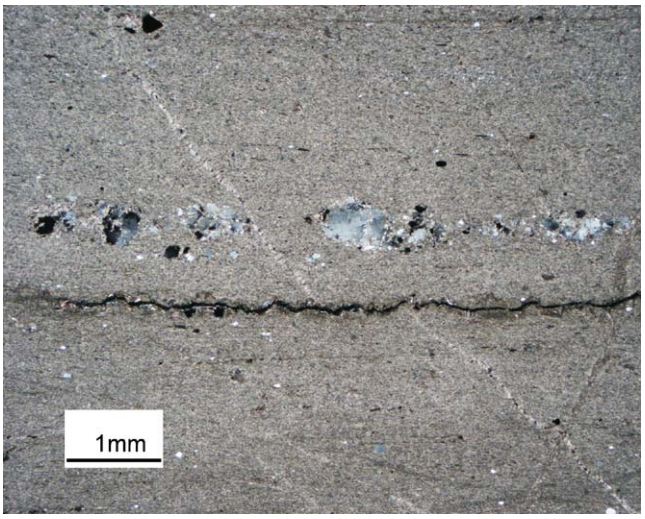

Fig. 6. Photomicrograph of apparent offset of small veins along stylolites demonstrating that pressure solution is not balanced by precipitation in form of fibrous veins (UTM 32 coordinates: Easting: 698 927 m Northing: 5 214 718 m, view to S).

for a given S, the maximum/minimum of Γ is dependent on S when located at higher A_k values with increasing strain (e.g. $A_k > 0.8$ for $S > 3$).

Fig. 4d is a plot exploring the dependence of ΔA on A_k, highlighting the trivial fact that the limits in area decrease are set limited by the point of complete loss of the material, whereas area increase has theoretically no limit:

$$\Delta A = e^{A_k S} \tag{12}$$

By definition, all curves for different S cross the origin of the plot where ΔA and A_k is zero. If A_k approaches -1, ΔA equals the exponent of $-S$.

4. Discussion

In the following section, we quantitatively examine a natural example with non-isochoric deformation with convergent transcurrence ($A < 0$). After a description of the geological setting, deformation parameters are deduced from our natural example involving pressure solution. The significance of this analysis is that the approach is applicable to other cases of convergent or divergent non-isochoric deformation in natural situations, such as soft-sediment deformation, shear zone development or deformation band formation.

4.1. Pressure solution

Pressure solution and stress-induced solution diffusive mass transfer may produce dark seams of insoluble material along dissolution surfaces that may have planar, wavy or sutured appearance (Engelder and Marshak, 1985). Discrete solution surfaces originate at sites of stress concentration and propagate through rock as anticracks (Fletcher and Pollard, 1981). Dissolution surfaces with narrow teeth normal or oblique to the surface are called stylolites and slickolites, respectively. The teeth are considered to be parallel to the direction of maximum compressive stress (Stockdale, 1922). Material is dissolved from sites of greater normal compressive stress and precipitated at sites of lesser stress although strain may also conceivably contribute to solution (Durney, 1972). If solution of material is not balanced by precipitation, the rocks experience volume loss. If heterogeneous deformation along narrow regularly spaced solution surfaces is present within an otherwise homogeneous greater area, the deformation can be integrated and approximated as homogeneous flow (Wojtal, 1989) and Eq. (6b) with $A < 0$ may be used to quantify the flow kinematics. Furthermore, if the rotational components of the finite deformation are small the orientation of the stress ellipsoid can be determined by measuring the orientation of the slickolites or the orientations of dissolution surfaces (Engelder and Marshak, 1985). If W_k can be derived from the orientation of the ISA with respect to the flow plane (i.e. an approximation of the fabric attractor) and if the percent ΔA can be estimated from dissolved markers (Ramsay and Huber, 1983), A_k (Eq. (5)) and S (Eq. (10)) can be calculated.

4.2. Natural example

To demonstrate an application of the convergent non-isochoric deformation tensor in nature we quantitatively describe ultra-mylonitic marble horizons from lower greenschist facies shear zones from the western Tauern Window (Tyrol/Austria). The examined shear zones crop out in the Zillertal Alps in the eastern Vals valley some 1.5 km North of the Geraer hut (UTM 32 coordinates: Easting: 698 927 m Northing: 5 214 718 m). These shear zones that are assumed to show plane strain deformation, define the boundary between the Zentralgneis (crystalline basement) and the overlying parautochthonous Lower Schieferhülle (Frisch, 1975) and record a W directed normal movement kinematically related to the N–S striking, W-dipping Brenner Normal Fault (Behrmann, 1988; Selverstone, 1988; Ebner, 2004). The ultramylonite marbles belong to a set of normal faults that are localized in the Hochstegen marble, located at the basal unit of the Lower Schieferhülle (Höck, 1969; Frisch, 1975). The shear zones have thicknesses of 5–30 cm and consist of impure marble ultra-mylonites containing white mica, quartz, and opaque phases (mainly Fe-oxides and sulfides). The host-rocks of these shear zones are made up of coarse-grained polygonal equigranular recrystallized marbles (crystal size ranges from 1 to 5 mm) that show no evidence of greenschist facies deformation.

Here, we focus on the latest deformation increment of the mylonites; a deformation that is accommodated by pressure solution localized along concentrated foliation-parallel surfaces these solution seams are confined to the interiors of the shear zone and cannot be found in the host rock. The pressure solution surfaces are highly indented consisting of interlocking teeth of wall rock. The teeth of these slickolites

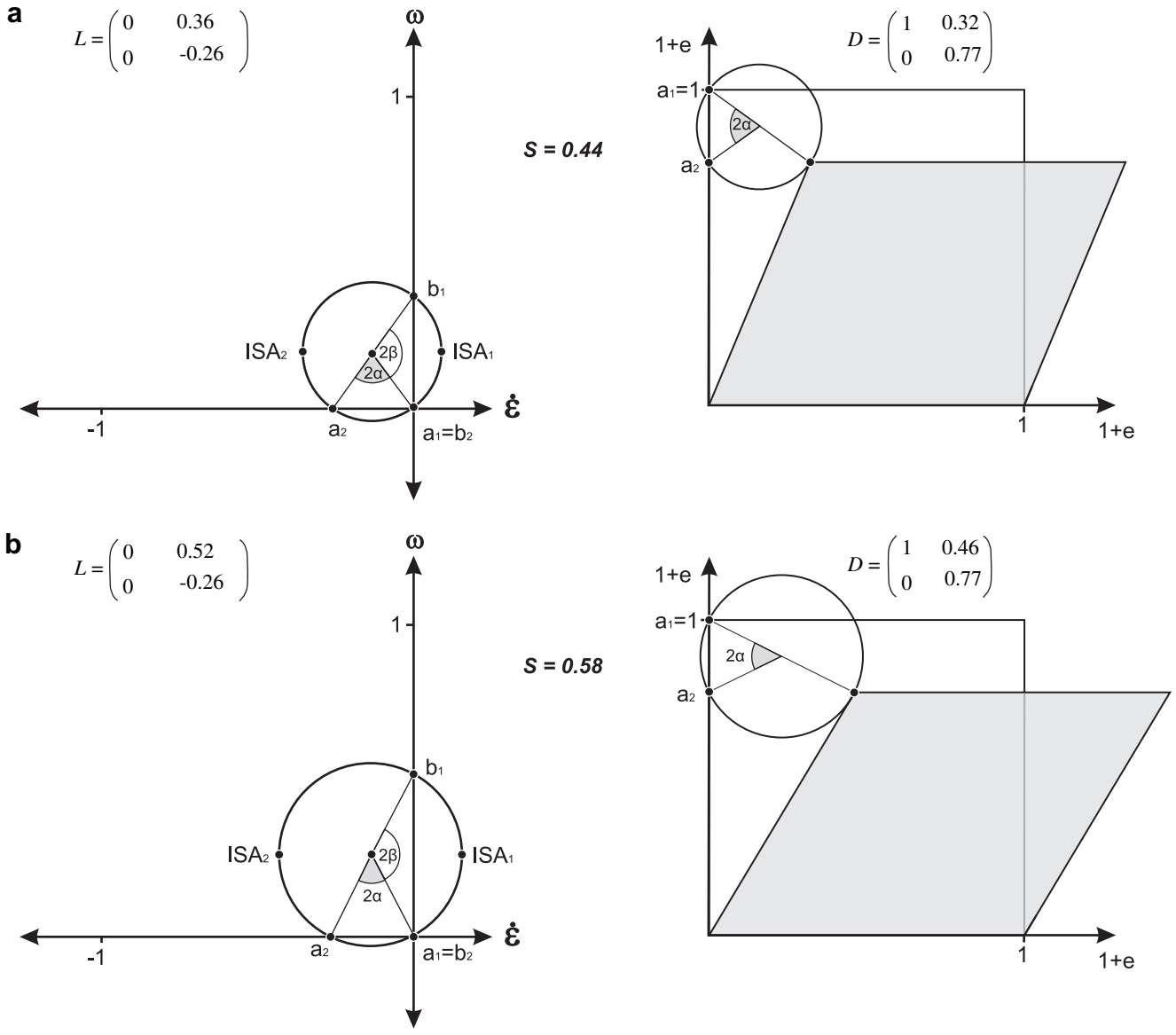

Fig. 7. Mohr circles of the velocity gradient tensor $\boldsymbol{L}$ (left column) as derived from the examined shear zones. The matching finite deformation tensors $\boldsymbol{D}$ and the finite deformation of a unit square (right column) were calculated using Eq. (8) under the precautious assumption of a correct amount of average volume loss $\Delta A = 23\%$ and the corresponding differential stretching rate S. (a) corresponds to Fig. 5a ($W_k = 0.81$; $A_k = -0.59$) (b) corresponds to Fig. 5b ($W_k = 0.89$; $A_k = -0.45$). See text for further description.

(Hancock, 1985) are inclined at about $60° \pm 5°$ (compare Fig. 5a and b) and are interpreted to have formed by dissolution along the pre-existing mylonitic foliation, the pressure solution seams record both shear displacement and shortening. Although the slickolites are discrete surfaces, they form penetrative 2–4 mm spaced cleavage domains throughout the shear zones and therefore we are confident that the deformation over the whole thickness of the shear zone can be regarded as homogeneous. Microstructural investigations reveal that the volume loss associated with the slickolites solution transfer cannot be balanced by precipitation volume gain associated with surrounding veins (Fig. 6) and therefore the shear zone in this stage of deformation experienced volume loss (Ebner, 2004). We conclude that, based on the microstructural investigations, the solution mass transfer accumulated deformation can be adequately described by convergent non-isochoric deformation.

Several quantitative kinematic studies have been proposed to establish the ratio of pure to simple shear (i.e. W_k), many of which are still in the phase of development (for a review see Ramsay and Lisle, 2000 and Passchier and Trouw, 2005). Here, we use the orientations of the teeth of the slickolites, measured in thin sections cut parallel to the shearing plane (Fig. 5). We assume that the mylonitic foliation, which has been used for pressure solution, is parallel to the fabric attractor, i.e. to the non-stretching eigenvector a_1 of convergent non-isochoric deformation. Furthermore, we assume that the long axes of the teeth of the slickolites point in the

direction of the shortening ISA (e.g. Gratier et al., 2005). With this angular relationship, the orientation of the second, shortening eigenvector a_2 can be reconstructed (Fig. 5). The arcus cosine of the angle α between the eigenvectors gives the W_k. The average angle of $\alpha = 30^\circ \pm 5^\circ$ suggests that the deformation is simple shear dominated with $W_k = 0.87 \pm 0.05$ and using Eq. (5), $A_k = -0.5 \pm 0.07$.

To characterise the finite deformation (i.e. finite deformation tensor $\boldsymbol{D}$) of our natural example the numerical values of W, A and S need to be known. To convert W_k and A_k into W and A (Eqs. (2) and (3)), we used the amount of average area loss ΔA (Eq. (12)) as a second independent variable to obtain the differential stretching rate S. To estimate the amount of finite volume loss for the entire shear zone, we used the geometry of small markers, which show an apparent offset along the stylolites similar to that shown in Fig. 6. This calculation gives a rough estimate of area loss within the shear zone (assuming that pressure solution only occurred along the microscopically visible sites, i.e. stylolites), about 20–25% (Ebner, 2004). With the amount of volume loss, the differential stretching rate S can be calculated by rearranging Eq. (10) or Eq. (12) or by alternately plotting the values of A_k and ΔA in Fig. 4d. Finally, the corresponding finite deformation tensor $\boldsymbol{D}$ can be calculated substituting A and W in Eq. (8). $\boldsymbol{D}$ is presented for the examined shear zones in the form of a deformed unit square in Fig. 7.

The quantification of this natural example shows that the offset across the shear zone is mainly controlled by the shearing component, whereas the thinning component is a result of area (volume) loss, which is not balanced by a shear zone parallel stretching component.

5. Conclusions

The velocity gradients tensor $\boldsymbol{L}$ for convergent or divergent non-isochoric flow (with no elongation parallel to the flow plane) is a simple but useful tool in order to explore the parameters that influence the kinematic consequences of non-isochoric deformation. In two-dimensions, $\boldsymbol{L}$ can be fully described by two parameters: the differential stretching rate S, and either the kinematic vorticity W_k or the kinematic dilatancy A_k, which are directly dependent. Using quantitative kinematic techniques for estimating the ratio of pure and simple shear (i.e. W_k), a direct measure of A_k can be established in those cases where the flow can be described by convergent or divergent non-isochoric deformation. The kinematic directions of this special type of flow have the following characteristics. (i) An instantaneously non-rotating, non-stretching orientation (i.e. the eigenvector a_1 or fabric attractor) parallel to the flow plane (this is similar to simple shear). (ii) A second instantaneously non-rotating, shortening/stretching orientation (i.e. eigenvector a_2) that is inclined into/against the shearing direction for convergent/divergent non-isochoric deformation. (iii) An increase in non-isochoric flow component is always associated with an increase in the coaxial component of deformation.

If the kinematic vorticity and dilatancy number in natural examples with convergent or divergent non-isochoric deformation can be derived by quantitative kinematic indicators, the full deformation gradient tensor $\boldsymbol{D}$ can be calculated by independent estimates of volume loss.

Acknowledgements

We acknowledge support from the Austrian Science Foundation (FWF grant P15668 and P18823-N19). We appreciate thorough reviews and improvements on a previous version of the text by Haakon Fossen and Declan De Paor. M. A. Edwards and U. Exner are thanked for stimulating discussions.

References

Behrmann, J.H., 1988. Crustal-scale extension in a convergent orogen: the Sterzing-Steinach mylonite zone in the Eastern Alps. Geodinamica Acta 2, 63–73.

Bobyarchick, A.R., 1986. The eigenvalues of steady flow in Mohr space. Tectonophysics 122, 35–51.

Carosi, R., Montomoli, C., Visona, D., 2006. Extensional shear zones in the core of the Higher Himalayan crystallines (Bhutan Himalaya): evidence for extrusion? In: Law, R., Searle, M.P., Godin, L. (Eds.), Channel Flow, Ductile Extrusion and Exhumation of Lower-Mid Crust in Continental Collision Zones. Geological Society, London, Special Publications 268, 200–216.

De Paor, D.G., Means, W.D., 1984. Mohr circles of the First and Second Kind and their use to represent tensor operations. Journal of Structural Geology 6, 693–701.

Druguet, E., Passchier, C.W., Carreras, J., Victor, P., Den Brock, S., 1997. Analysis of a complex high-strain zone at Cap de Creus, Spain. Tectonophysics 280, 31–45.

Durney, D.W., 1972. Solution-transfer, an important geological deformation mechanism. Nature 235, 315.

Ebner, M., 2004. Deformation in the Footwall of the Brenner Normal Fault: Normal Versus Strike-Slip Faulting. Unpublished Diploma thesis, University of Vienna.

Engelder, T., Marshak, S., 1985. Disjunctive cleavage formed at shallow depths in sedimentary rocks. Journal of Structural Geology 7, 327.

Fletcher, R.C., Pollard, D.D., 1981. Anticrack model for pressure solution surfaces. Geology 9 (9), 419–424.

Fossen, H., Tikoff, B., 1993. The deformation matrix for simultaneous simple shearing, pure shearing and volume change, and its application to transpression transtension tectonics. Journal of Structural Geology 15 (3–5), 413–422.

Frisch, W., 1975. Ein Typ-Profil durch die Schieferhülle des Tauernfensters: das Profil am Wolfendorn (westlicher Tuxer Hauptkamm, Tirol). Verhandlungen der Geologischen Bundesanstalt 2–3, 201–221.

Ghosh, S.K., Ramberg, H., 1976. Reorientation of inclusions by combination of pure shear and simple shear. Tectonophysics 34 (1–2), 1–70.

Grasemann, B., Edwards, M.A., Wiesmayr, G., 2006. Kinematic dilatancy effects on orogenic extrusion. In: Law, R., Searle, M.P., Godin, L. (Eds.), Channel Flow, Ductile Extrusion and Exhumation of Lower-Mid Crust in Continental Collision Zones. Geological Society, London, Special Publications 268, 183–199.

Grasemann, B., Fritz, H., Vannay, J.-C., 1999. Quantitative kinematic flow analysis from the Main Central Thrust Zone (NW-Himalaya, India); implications for a decelerating strain path and the extrusion of orogenic wedges. Journal of Structural Geology 21, 837–853.

Gratier, J.P., Muquet, L., Hassani, R., Renard, F., 2005. Experimental microstylolites in quartz and modeled application to natural stylolitic structures. Journal of Structural Geology 27, 89–100.

Hancock, P.L., 1985. Brittle microtectonics: principles and practice. Journal of Structural Geology 7, 437–457.

Höck, V., 1969. Zur Geologie des Gebietes zwischen Tuxer Joch und Olperer (Zillertal, Tirol). Jahrbuch der Geologischen Bundesanstalt 112, 153–195.

Holcombe, R.J., Little, T.A., 2001. A sensitive vorticity gauge using rotated porphyroblasts, and its application to rocks adjacent to the Alpine Fault, New Zealand. Journal of Structural Geology 23, 979–989.

Law, R., Searle, M.P., Simpson, R.L., 2004. Strain, deformation temperatures and vorticity of flow at the top of the Greater Himalayan Slab, Everest Massif, Tibet. Journal of the Geological Society of London 161, 305–320.

Lister, G.S., Williams, P.F., 1983. The partitioning of deformation in flowing rock masses. Tectonophysics 92, 1–33.

Marrett, R., Peacock, D.C.P., 1999. Strain and stress. Journal of Structural Geology 21, 1057–1063.

Passchier, C.W., 1987. Stable positions of rigid objects in non-coaxial flow – a study in vorticity analysis. Journal of Structural Geology 9, 679–690.

Passchier, C.W., 1988. Analysis of deformation paths in shear zones. Geologische Rundschau 77, 309–318.

Passchier, C.W., 1991. The classification of dilatant flow types. Journal of Structural Geology 13, 101–104.

Passchier, C.W., Mancktelow, N.S., Grasemann, B., 2005. Flow perturbations: a tool to study and characterize heterogeneous deformation. Journal of Structural Geology 27, 1011–1026.

Passchier, C.W., Trouw, R.A.J., 2005. Microtectonics. Springer-Verlag, Berlin.

Platt, J.P., Behrmann, J.H., 1986. Structures and fabrics in a crustal-scale shear zone, Betic Cordillera, SE Spain. Journal of Structural Geology 8, 15–33.

Provost, A., Buisson, C., Merle, O., 2004. From progressive to finite deformation and back. Journal of Geophysical Research 109, B02405, doi:10.1029/2001JB001734.

Ramsay, J.G., Huber, M.I., 1983. The Techniques of Modern Structural Geology. In: Strain Analysis, vol. 1. Academic Press Inc. Ltd, London.

Ramsay, J.G., Huber, M.I., 1987. The Techniques of Modern Structural Geology. In: Folds and Fractures, vol. 2. Academic Press Inc. Ltd, London.

Ramsay, J.G., Lisle, R.J., 2000. The Techniques of Modern Structural Geology. In: Applications of Continuum Mechanics in Structural Geology, vol. 3. Academic Press Inc. Ltd, London.

Ring, U., 1998. Volume strain, strain type and flow path in a narrow shear zone. Geologische Rundschau 86, 786–801.

Ring, U., Brandon, M.T., Ramthun, A., 2001. Solution-mass-transfer deformation adjacent to the Glarus Thrust, with implications for the tectonic evolution of the Alpine wedge in eastern Switzerland. Journal of Structural Geology 23, 1491–1505.

Schwerdtner, W.M., 1982. Calculation of volume change in ductile band structures. Journal of Structural Geology 4, 57–62.

Selverstone, J., 1988. Evidence for east–west crustal extension in the eastern Alps: implications for the unroofing history of the Tauern Window. Tectonics 7, 87–105.

Simpson, C., De Paor, D.G., 1997. Practical analysis of general shear zones using the porphyroclast hyperbolic distribution method: an example from the Scandinavian Caledonides. In: Sengupta, S. (Ed.), Evolution of Geological Structures in Micro- to Macro-scales. Chapman & Hall, London, pp. 169–184.

Stockdale, P.B., 1922. Stylolites: their nature and origin. Indiana University Studies 9, 1–97.

Sturm, R., 2003. SHEARCALC – a computer program for the calculation of volume change and mass transfer in a ductile shear zone. Computers & Geosciences 29, 961–969.

Tikoff, B., Fossen, H., 1993. Simultaneous pure and simple shear – the unifying deformation matrix. Tectonophysics 217 (3–4), 267–283.

Truesdell, C., 1954. The Kinematics of Vorticity. Indiana University Press, Bloomington, Indiana.

Vissers, R.L.M., 1989. Asymmetric quartz *c*-axis fabric and flow vorticity: a study using rotated garnets. Journal of Structural Geology 11, 231–244.

Wallis, S.R., 1992. Vorticity analysis in a metachert from the Sanbagawa Belt, SW Japan. Journal of Structural Geology 14, 271–280.

Wallis, S.R., 1995. Vorticity analysis and recognition of ductile extension in the Sanbagawa belt, SW Japan. Journal of Structural Geology 17, 1077–1093.

Wojtal, S., 1989. Measuring displacement gradients and strains in faulted rocks. Journal of Structural Geology 11 (6), 669–678.

Wright, T.O., Platt, L.B., 1982. Pressure dissolution and cleavage in the Martinsburg Shale. American Journal of Science 282 (2), 122–135.